Journal of the European Ceramic Society **5** (1989) 269–281

The Effect of Iron Diffusion into a Glass-Ceramic Coating on Mild Steel—a Bulk Glass Simulation

F. Sun* & D. Holland‡

Centre for Advanced Materials Technology, Physics Department, University of Warwick, Coventry CV4 7AL, UK

(Received 31 July 1989; accepted 27 September 1989)

Abstract

Earlier work demonstrated that extensive iron diffusion can occur during the coating of a mild steel substrate with a lithium silicate glass-ceramic. This resulted in a composition gradient in the coating which had profound effect on the crystallisation process. By studying bulk glasses of compositions along this profile, the authors have related composition to phase and microstructure development in the coating and shown that a deleterious thermal expansion profile is created. These effects can be explained in terms of the relative content of Fe(II), Fe(III), P_2O_5 and K_2O arising from the interdiffusion process. A lithium (zinc, iron) silicate solid solution phase is reported.

Frühere Arbeiten haben gezeigt, daß während der Beschichtung eines Flußeisensubstrates mit einer Lithium-Silikat-Glaskeramik eine ausgeprägte Eisendiffusion auftreten kann. Das führt zu einem Gradienten in der Zusammensetzung der Beschichtung, der einen großen Einfluß auf den Kristallisationseffekt hat. Durch das Studium kompakter Gläser, die Zusammensetzungen entlang des Konzentrationsprofils aufweisen, konnte die Zusammensetzung mit der Phasenentwicklung und der mikrostrukturellen Entwicklung in der Beschichtung in Beziehung gesetzt werden. Außerdem konnte gezeigt werden, daß ein ungünstiges Profil der thermischen Ausdehnung erzeugt wird. Dieser Effekt kann durch die relativen Gehalte an Fe(II), Fe(III), P_2O_5 und K_2O, die sich durch den Interdiffusionsprozeß ergeben, erklärt werden. Es wird außerdem eine Lithium (Zink, Eisen) Silikat-Mischkristallphase beschrieben.

Des travaux antérieurs ont montré que le fer diffuse fortement lors du dépôt d'une vitrocéramique de silicate de lithium sur un substrat d'acier doux. Celà provoque dans le dépôt un gradient de composition qui influence profondément la cristallisation. En étudiant des verres de compositions choisies le long de ce profil, nous avons relié la composition au développement des phases et de la microstructure dans le dépôt, et montré qu'il se forme un profil d'expansion thermique préjudiciable. Ces effets peuvent être expliqués par les teneurs relatives en Fe(II), Fe(III), P_2O_5 et K_2O provenant du processus d'interdiffusion. On décrit également une solution solide de silicate de lithium contenant du zinc et du fer.

1 Introduction

The requirement for inorganic coatings, either vitreous or ceramic, on metal substrates is of significant technological importance. Such coatings provide metals with many improved properties, such as resistance to oxidation, chemical corrosion, abrasion, or the provision of a thermal or an electrical barrier, etc. Therefore, inorganic coatings have been widely used not only in the traditional enamelling industry but in modern technology as well.[1,2]

The beneficial properties of the coating depend on its good adhesion to the metal substrate and a suitable value of stress at the coating–metal interface. The adhesion of coatings is due to chemical as well as mechanical bonding and it is generally believed that the metal oxide at the coating–metal interface is a critical factor for chemical bonding. Thus, the interaction between the coating and the oxide will have considerable influence on coating properties. In addition, a close

* Visiting professor from the East China Institute of Chemical Technology, 130 Mei-Loung Road, Shanghai, People's Republic of China.
‡ To whom all correspondence should be addressed.

Journal of the European Ceramic Society 0955-2219/90/$3.50

matching of thermal expansion coefficients of the coating and the metal is necessary to avoid excessive stress generation at the interface.[1,3,4]

Glass-ceramic coatings have some advantages over vitreous or ceramic coatings. Their combination of mechanical strength, hardness and refractoriness, with easy control of the thermal expansion, prove them to be attractive coating materials and they have increasingly widespread usage. Several glass-ceramic coatings based on Li_2O–Al_2O_3–SiO_2 and Li_2O–B_2O_3–SiO_2 systems have been developed for mild steel to provide protection from oxidation and corrosion. It is a composition from the former system which is considered here.[5]

With the aim of improving the properties and extending the usage of glass-ceramic coatings, a series of studies have been carried out on the interactions at the coating–metal interface, examining the dissolution and diffusion of various metal ions and their effects on the crystallisation as well as the adhesion of glass-ceramic coatings.[5,6] It has been observed in previous work that two kinds of substrate, a 17% chrome–iron alloy and a low carbon (<0·01% C) mild steel exhibited very different effects on being coated with nearly identical lithium aluminosilicate compositions.[5,6] In the case of the chrome–iron alloy, the interfacial Cr_2O_3 layer showed only low dissolution into the glass-ceramic coating, resulting in little effect on the microstructure of the adjacent coating whilst producing an oxide-saturated transition layer for good adhesion. For mild steel, owing to the high solubility and mobility of FeO, iron diffused rapidly into the coating, producing a high iron concentration adjacent to the interface which had a major influence on the kinds of crystal phases precipitated and the microstructure of the resulting ceramic coating. For a detailed appreciation of the consequences of coating mild steel with a lithium silicate-type glass-ceramic, the influence of ferrous oxide on the crystallisation behaviour and the properties of the glass-ceramic coating need to be known. Limited information is available from the coating composition profile.[5,6] The present work discusses the crystallisation behaviour and relevant physical properties of bulk glasses which have compositions corresponding to the different layers in the coating composition profile.

Table 1. Glass compositions[a] (wt%)

Sample	*Distance to the interface*	*Al_2O_3*	*SiO_2*	*P_2O_5*	*K_2O*	*ZnO*	*Li_2O*	*FeO*
B1	2–10 μm	3·4	55·6	2·1	0·9	4·4	8·7	24·7
B2	10–18 μm	3·5	57·0	1·1	1·5	3·4	8·9	24·5
B3[b]	18–26 μm	2·9	57·1	1·3	4·3	0·0	8·9	22·7
B4	26–34 μm	3·2	60·4	1·5	5·2	1·7	9·5	18·6

[a] These glass compositions were obtained from the quantitative EDX analysis of the glass-ceramic coating profile with the assumption that the ratio of lithium to silicon in the profile glass was the same as that in the parent glass.
[b] B3 glass was prepared without the ZnO component to assess the effect of volatilisation of this oxide.

2 Experimental Procedure

2.1 Glass compositions

Four glass compositions were chosen for investigation. Three of these (B1, B2, B4) corresponded to points on the composition profile of a glass-ceramic coating based on the lithium aluminosilicate system adjacent to the interface with a mild steel substrate. An additional composition (B3) was prepared without the ZnO component to assess the effect of volatilisation of this oxide. All glass compositions are shown in Table 1.

These glass compositions were obtained from the quantitative EDX analysis of the glass-ceramic coating profile shown in Fig. 1, using the arbitrary assumption that the ratio of lithium to silicon throughout the profile remained the same as that in the parent glass.

2.2 Glass preparation

Glass batches of 120 g were made up using 'Analar' grade reagents, consisting of SiO_2, Al_2O_3, $AlPO_4$,

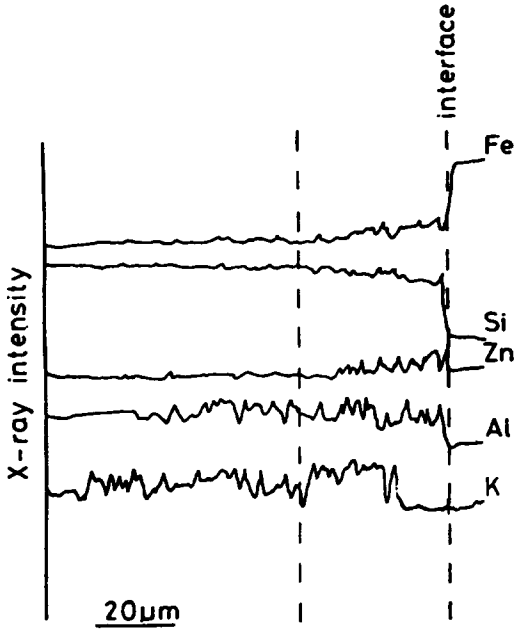

Fig. 1. Element distribution collected from line scans conducted across the interface.

$FeC_2O_4 . 2H_2O$, Li_2CO_3, K_2CO_3 and ZnO, and then homogenised by tumble-rolling. The batch was first poured into a platinum 10% rhodium crucible which was then covered with a platinum lid and transferred into a vertical electrical tube furnace. Oxygen-free N_2 was used to flow in the top of the furnace where the gap was sealed by high temperature cement to keep the inside airtight. Contact with oxygen was minimised to suppress oxidation of Fe^{2+} to Fe^{3+} as far as possible. The furnace was then heated from room temperature to 1350°C and held for 1 h. Most of the melt was cast into a glass block while the rest was quenched into deionised water to form frit. The bulk glasses were annealed in an electrical furnace at 400°C for 1 h followed by slow cooling in the furnace. The bulk glasses were cut into slices of about 30 mm × 8 mm × 4 mm for further investigation.

Some melts were wholly quenched to a frit, then crushed in a tool-steel mortar, mixed thoroughly and remelted as above in an attempt to improve the homogeneity of glass. However, the remelting usually resulted in a decrease of the Fe(II)/Fe(III) ratio.

2.3 Heat treatment

A two-stage heat treatment schedule (Fig. 2) as used in previous work[5,6] was selected for the crystallisation of bulk glasses in order to make comparison with the crystallisation behaviour of the coating on mild steel.

To prevent further oxidation, all heat treatments were carried out under an atmosphere of O_2-free N_2.

2.4 Differential thermal analysis (DTA)

A differential thermal analysis (DTA) study was undertaken so that the temperature range of exothermic crystallisation on reheating the glass powders could be observed. About 200 mg of sample was loaded in a platinum pan, and heated to ~1050°C at a rate of 8°C/min. The DTA runs were made in N_2 atmosphere, and silica powder was used as a standard reference material. Some DTA runs were terminated after a particular exothermic event, and the cooled specimens were analysed by XRD in order to identify the crystalline species associated with that thermal event. To investigate the influence of nucleation on high temperature crystallisation, some DTA runs were carried out using glass powder preheated at a temperature ranging from 500 to 580°C for 3 h.

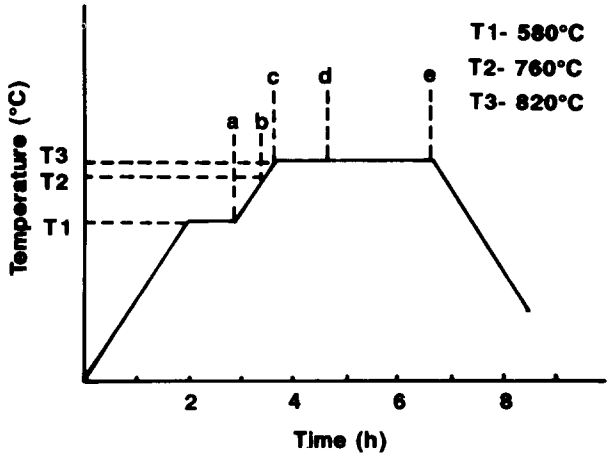

Fig. 2. Heat treatment schedule.

2.5 Identification of crystal phases

X-ray diffraction analysis (XRD) was undertaken using a Philips powder diffractometer to identify the crystal phases present before and after different stages of heat treatment. Monochromatised CuK_α radiation was used in all runs.

2.6 Examination of microstructure

All samples, after different stages of heat treatment, were cut in cross-sections which were then mounted in bakelite and polished to a 1 μm finish. After being coated with carbon, the microstructures of some samples were examined by back-scattered imaging using a Cambridge scanning electron microscope. The relative distribution of constituent elements was obtained by an energy dispersive X-ray analysis (EDX). A beam current of 3×10^{-12} A, an accelerating voltage of 20 kV, and a sampling period of 100 s were used in spot analysis. Treatment of the collected X-ray spectrum allowed full quantitative analysis of all detectable elements except oxygen and lithium.

2.7 Measurement of thermal expansion coefficient

The coefficients of thermal expansion of the samples of $4 \times 5\,mm^2$ cross-section and 30 mm long were measured with a fused silica dilatometer, before and after different stages of heat treatment.

2.8 Determination of the ferrous/ferric ration in glass

The ferrous/ferric ratios in the glasses were determined using a spectrophotometric method.[8]

The fraction of Fe(III) was evaluated using the relationship Fe(III)/Fe(total) = absorbance before addition of ammonium persulphate/absorbance after addition of ammonium persulphate. The fraction of Fe(II) could then be obtained by difference.

3 Results

3.1 Fe(II)/Fe(total) ratio

The real Fe(II)/Fe(total) ratios of the high-iron-content Li_2O–Al_2O_3–SiO_2 glasses, the nominal compositions of which are listed in Table 1, are shown in Table 2. It can be seen that although $FeC_2O_4 . 2H_2O$ was selected as a starting material and an O_2-free N_2 atmosphere was used, the tendency for Fe(II) to be oxidised was still considerable, indicating that there was some air leakage.

3.2 DTA scans of glasses

Figure 3 is a composite plot of the DTA scans run at 8°C/min for all iron-containing glasses, together with that for B glass which was the parent glass for the glass-ceramic coating.

The DTA scans for these four iron-containing glasses are similar, but quite different from that for glass B. The first endothermic peaks corresponding to the glass transition are observed in the temperature range of 440 to 457°C. There exist four exothermic peaks for all iron-containing glasses compared with only two for B glass. The temperatures of the exothermic peak maxima are marked on Fig. 3 and the crystallised phases associated with the exothermic events are listed in Table 3. It can be seen from Table 3 that the first, third and fourth exotherms are associated with the crystallisation of the same kind of phases, i.e., the first exotherm is due to the precipitation of a lithium zinc iron silicate solid solution with the general formula $Li_2Zn_xFe_{(1-x)}SiO_4$, known as L(ZF)Sss, and the fourth exotherm is associated with the crystallisation of $LiFeSi_2O_6$ (LF_2S_4), as confirmed by XRD and EDX. Although the product of the third exotherm has not been fully characterised, it is likely to be an iron silicate (FS), and probably associated with Fe(III). It is interesting to note the different crystallised phases associated with the second exotherm. For B1 and B2, quartz precipitated as a second crystalline phase, though the second exotherm for B2 is rather low compared with that of B1, whereas $Li_2O . SiO_2$ (LS) appears with the second exotherm for B3 and B4. It is notable that $Li_2O . 2SiO_2$ (LS_2), the first crystallised phase for B glass, has not been found during the devitrification

Table 2. Fe(II)/Fe ratios

Glass no.[a]	B1	B1′	B2	B3	B4
Fe(II)/Fe ratio (%)	58·6	40·5	59·8	62·8	61·2

[a] B1′ glass was obtained by quenching B1 melt completely to a frit, and melting again.

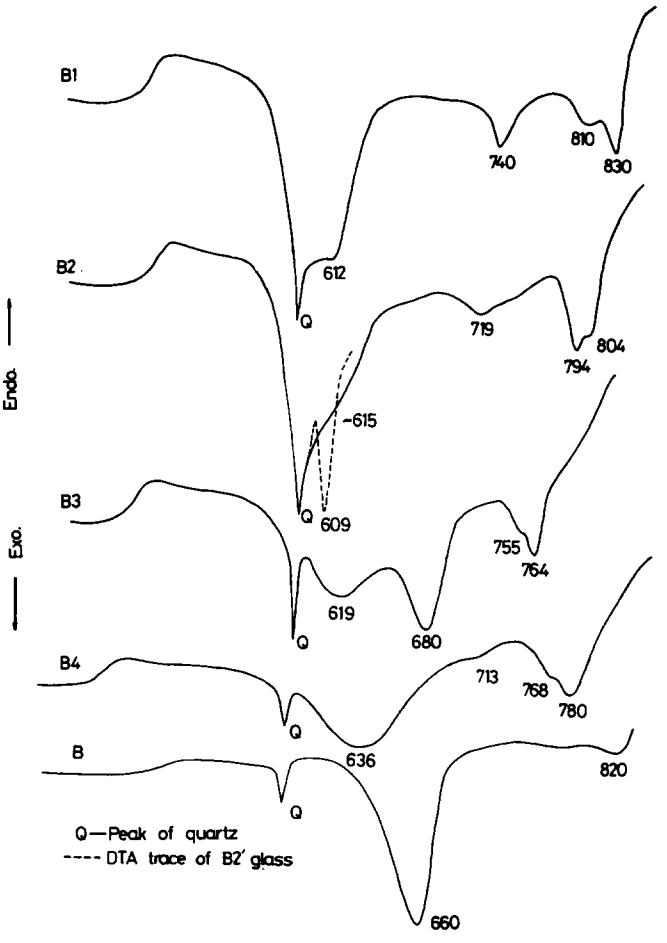

Fig. 3. Composite plot of DTA scans, each run at 8°C/min, for all iron-containing glasses, together with that for B glass which was the parent glass for the glass-ceramic coating.

of the iron-containing glasses. It is also noticeable that a small amount of quartz appears after DTA runs for B3 and B4 glasses, but it is difficult to associate it with any particular exotherm at this time.

A group of DTA scans was run for B1 samples heated previously in the temperature range from 530 to 580°C. The results are shown in Fig. 4. A distinct

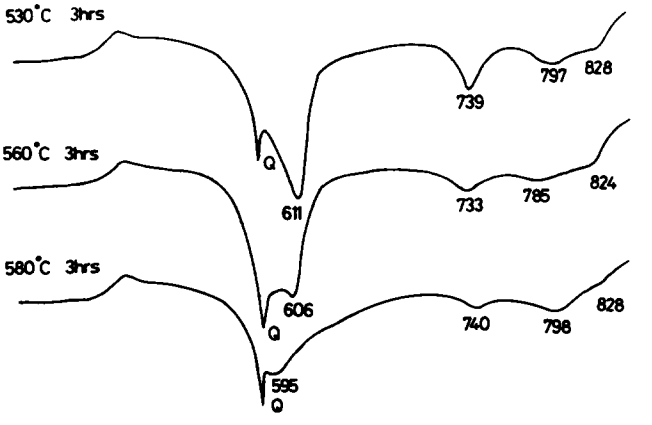

Fig. 4. DTA traces for B1 glass heat treated previously at the temperatures shown for 3 h.

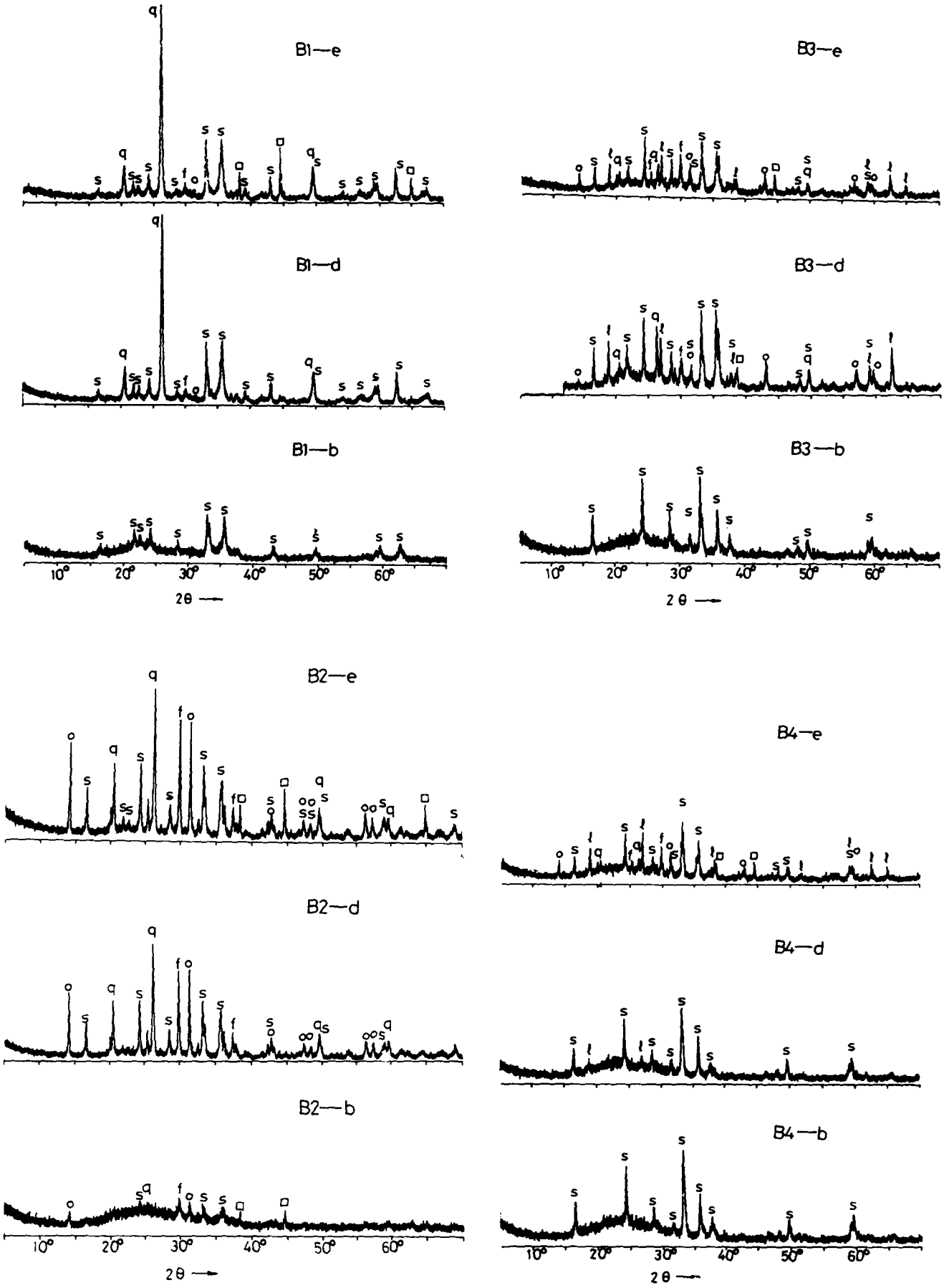

Fig. 5. XRD patterns for iron-containing glasses after different stages of heat treatment: s, L(ZF)Sss; q, quartz; l, LS; f, FS; o, LF_2S_4 □, Al(holder).

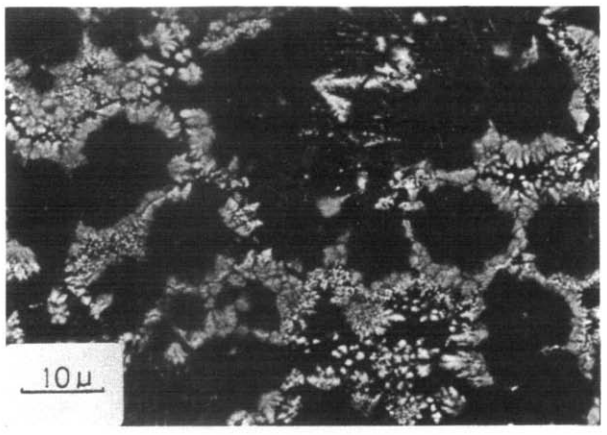

B1—e

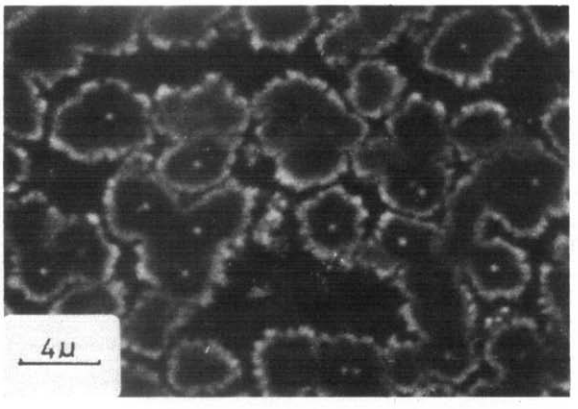

B1—b

(a)

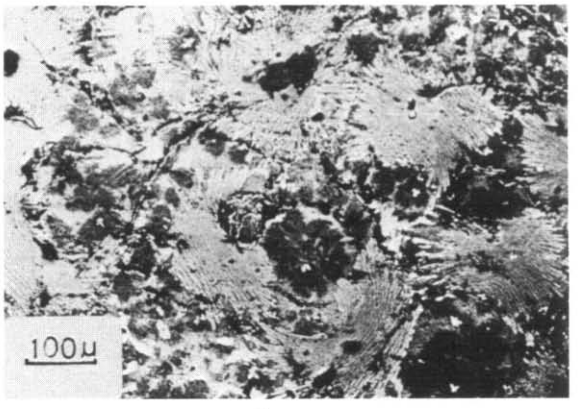

B2—e

B2—e

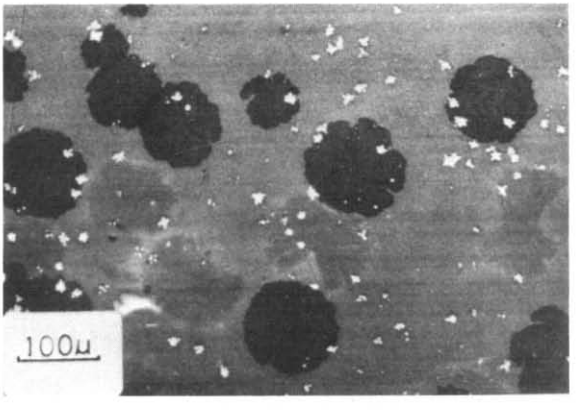

B2—b

(b)

Fig. 6. Back scattered electron micrographs for iron-containing glasses after different stages of heat treatment: (a) B1-e (580°C, 1 h; 820°C, 3 h), B1-b (580°C, 1 h; 760°C, zero hold); (b) B2-e (580°C, 1 h; 820°C, 3 h), B2-b (580°C, 1 h; 760°C, zero hold).

decrease of the temperature of the first exothermic maximum can be observed.

3.3 Crystallisation and microstructure

The sequence of crystallisation for all iron-containing glasses during heat treatment, as determined by X-ray diffraction, SEM investigation and EDX analysis, are not as predicted by the DTA results. The XRD patterns of B1, B2, B3, B4 glasses crystallised at different stages of heat treatment are compared in Fig. 5. The corresponding SEM micrographs are shown in Fig. 6, and the phases present are summarised in Table 4.

For B1 sample heat treated at 580°C for 1 h the XRD pattern and SEM micrograph show no appreciable evidence for the existence of any crystalline phase. However, a set of peaks, which is similar to those of lithium zinc silicate (Li_2ZnSiO_4)

Table 3. Relationship between temperature of exothermic maximum and corresponding crystalline phase precipitated

Sample	*L(ZF)Sss*[a]	LS_2	*Quartz*	*LS*	*FS*[b]	LF_2S_4[c]
B1	612	—	740	—	810	830
B2	~615	—	719	—	794	804
B3	619	—	tr[d]	680	755	764
B4	636	—	tr[d]	713	768	780
B	—	660	820	—	—	—

[a] L(ZF)Sss = Lithium iron zinc silicate solid solution.
[b] FS = a kind of iron silicate.
[c] $LF_2S_4 = LiFeSi_2O_6$.
[d] In B3 and B4 glasses, a small proportion of quartz is also present, but it is not clear with which peak it is associated.

B3—e

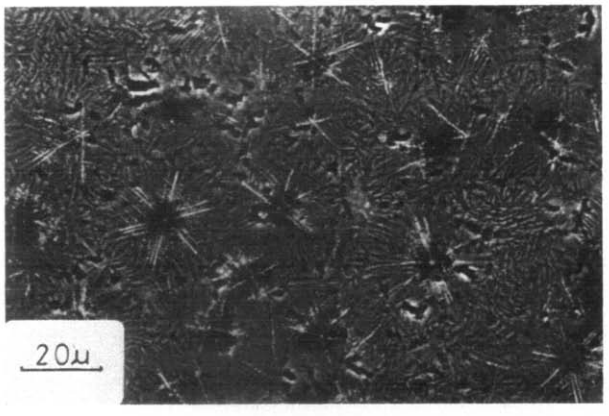

B3—c

(c)

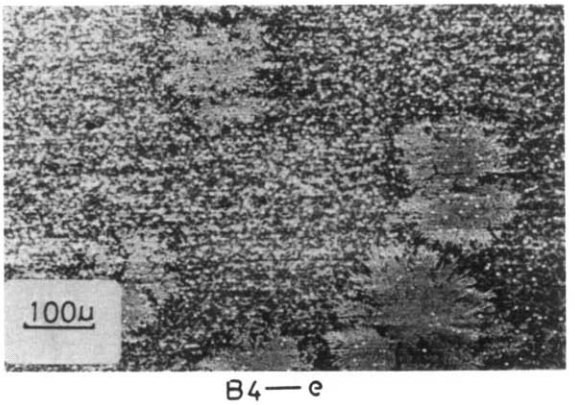

B4—e

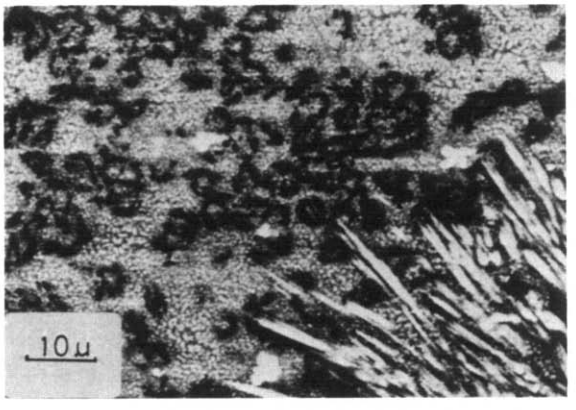

B4—e

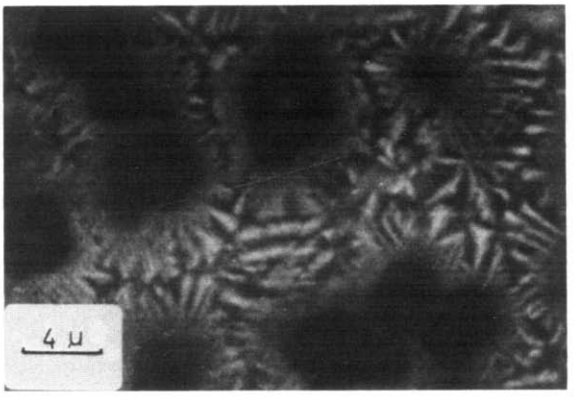

B4—b

(d)

Fig. 6—*contd.* (c) B3-e (580°C, 1 h; 820°C, 3 h), B3-c (580°C, 1 h; 820°C, zero hold); (d) B4-e (580°C, 1 h; 820°C, 3 h), B4-b (580°C, 1 h; 760°C, zero hold).

but slightly shifted, is observed in the XRD pattern when the temperature reaches 760°C (Fig. 5). In fact, these peaks can be fitted very well to a $Li_2Zn_xFe_{(1-x)}SiO_4$ solid solution, L(ZF)Sss. Quartz formation is also apparent but to a lesser degree. A small amount of FS and LF_2S_4 are eventually observed in B1 samples crystallised at 820°C when the time extends to 3 h (Fig. 5). The back-scattered electron micrograph (Fig. 6) shows that the dark circular areas, the diameters of which have increased to about 10–20 μm, have given rise to more coherent radial grey dendritic crystals. The annular bright dendrites, which appear to have better defined crystallinity than in the case of 760°C, seem to be the extension of the internal radial grey dendrites. EDX analysis shows no significant difference in the composition, either in the radial grey dendrite areas or in the bright dendrites, between B1 samples heat treated at 760°C with zero hold and that at 820°C for 3 h.

Although XRD shows that one of the main crystalline phases is quartz, its crystallites are too small to be identified by SEM. Comparing the results of XRD and EDX, it is reasonable to suggest that the crystallites are embedded in the dendrites as well as the glass matrix.

The crystallisation behaviour of B2 glass is different from that of B1 glass. No detectable peak is found in the XRD pattern for B2 sample heat treated at 580°C for 1 h though L(ZF)Sss, quartz, FS and LF_2S_4 appear simultaneously in the B2 sample when the temperature reaches 760°C (Fig. 5). In the corresponding back-scattered electron micrograph

Table 4. Crystalline phases[a] precipitated during different stages of heat treatment

No.	Heat treatment schedule	B1		B2		B3		B4	
		Major CP	Minor CP	Major CP	Minor CP	Major CP	Minor CP	Major CP	Minor CP
A	580°C 1 h								
B	580°C, 1 h 760°C, zero hold	SS	Q	SS LF_2S_4 FS Q		SS		SS	
C	580°C, 1 h 820°C, 1 h	SS Q		Q SS LF_2S_4 FS		SS		SS	
D	580°C, 1 h 820°C, 1 h	Q SS	FS	Q LF_2S_4		SS LS	Q FS	SS	LS
E	580°C, 1 h 820°C, 3 h	Q SS	FS LF_2S_4	Q LF_2S_4 FS SS		SS LS FS LF_2S_4	Q	LS SS LF_2S_4 FS	Q

[a] Major CP = Major crystal phase, Minor CP = Minor crystal phase.

(Fig. 6), there are three kinds of visible crystals embedded separately in the glass matrix: the large spherulites, which consist of grey radial dendrites and dark matrix, are of the order of 100–200 μm, and the small bright dendrites of FS are of $\sim 10\,\mu$m, as deduced by the XRD and EDX analysis. However, quartz is still too small to be visible. More crystals of the four kinds precipitate and coarsen with increase of heat treatment temperature and time, resulting in a more crystallised and coarse-grained material (Fig. 6). The XRD patterns (Fig. 5) show that the peak heights related to quartz, LF_2S_4 and FS increase distinctly whereas those for L(ZF)Sss remain unchanged. It is noticeable that a number of cracks have developed in the B2 sample heat treated at 820°C for 3 h (Fig. 6).

As can be seen in Figs 5 and 6, the crystallisation behaviour of B4 glass in the initial stages of heat treatment is similar to B1 glass in that the only crystalline phase present is L(ZF)Sss when the temperature reaches 760°C. The dark spherulites, which are of the order of 3–5 μm and enriched in silicon and probably also lithium, are surrounded by the grey radial dendrites of L(ZF)Sss in both cases, and there exist bright cores of the order of $\sim 1\,\mu$m in some of the spherulites. L(ZF)Sss remains the unique crystalline phase until the temperature reaches 820°C. However, with extension of heat treatment, the development of crystallisation appears to be quite different from that of B1 glass. The dark cored crystals precipitate from the dark round areas, and the large sheaves of LF_2S_4 as well as small bright dendrites of FS also crystallise, giving three major crystalline phases in addition to L(ZF)Sss. Conversely, only small amounts of quartz are present. It is very interesting to note that the L(ZF)Sss dendrites have changed into small spherulites although there is no evidence of change in crystal phases.

The crystallisation process of B3 glass is similar to that of B4. The main differences are that, except for the dark LS dendrites, the bright FS dendrites also develop from the dark round areas. The FS phase is well crystallised, and the morphology of the L(ZF)Sss dendrites remains unchanged after heat treatment.

3.4 Thermal expansion characteristics of the iron-containing glasses before and after heat treatment

The thermal expansion coefficients of all iron-containing glasses before and after different stages of heat treatment are listed in Table 5.

It can be seen that there exists a slight decrease in the coefficient for B1 sample after nucleation, followed by a marked increase with increasing heat treatment temperature and time. This early decrease in coefficient extends to high temperatures for B2 glass then is followed by a more gradual rise with the extension of crystallisation. Heat treatment only has a relatively small effect upon the thermal coefficients for B3 and B4 glasses.

4 Discussion

4.1 Crystallisation of lithium iron silicate phases

The first question to be addressed is the occurrence of iron-containing silicates precipitated during crystallisation. As can be seen in Fig. 5, similar peaks

occur in the XRD patterns for all iron-containing glass-ceramics produced either from DTA runs terminated above the first exotherm or by heat treatment to 760°C. These peaks resemble those of Li_2ZnSiO_4, but EDX analysis indicates that the dendritic crystals contain far more iron than zinc. However, there is no information on such a phase in the JCPDS file. Therefore, synthetic lithium zinc iron silicates $Li_2Zn_{(1-x)}Fe_xSiO_4$ were prepared with different x values of 0·5, 0·75 and 1. The EDX analysis confirmed that the resulting materials consisted essentially of lithium zinc iron silicate solid solution $Li_2Zn_{(1-x)}Fe_xSiO_4$ (for $x = 0{\cdot}5$ or $x = 0{\cdot}75$) or Li_2FeSiO_4 (for $x = 1$), along with traces of LS and FeO. Their XRD patterns are illustrated in Fig. 7. It can be seen that the XRD patterns are similar to that of Li_2ZnSiO_4 and in good agreement with the XRD patterns of the iron-containing glasses after the first stage of crystallisation. There are some small deviations of the d-spacings of the peaks and also peak heights of the solid solution in the crystallised glasses from those of synthetic $Li_2Zn_{(1-x)}Fe_xSiO_4$. These can be interpreted as due to the wider range of and additional substitutions in the crystalline lattice

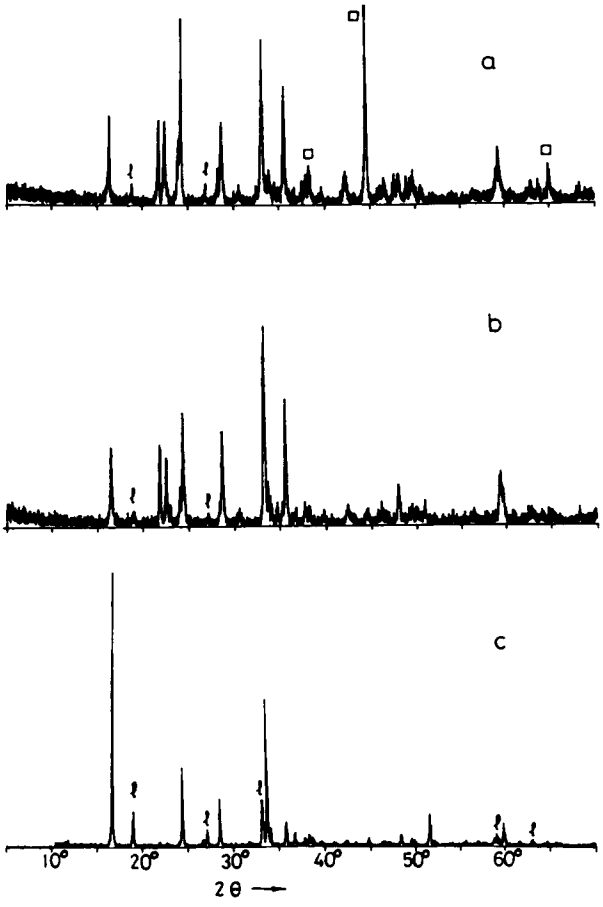

Fig. 7. XRD patterns of some synthetic lithium iron zinc silicate solid solutions: (a) $LiFe_{0{\cdot}5}Zn_{0{\cdot}5}SiO_4$; (b) $LiFe_{0{\cdot}75}Zn_{0{\cdot}25}SiO_4$; (c) $LiFeSiO_4$. l = LS, □ = Al(holder).

(e.g. Al^{3+} for Si^{4+} and so on) and the distortion of the crystal structure.

This result is also consistent with the previous work on the glass-ceramic coating[5,6] in which $Li_2Fe_{0{\cdot}8}Zn_{0{\cdot}2}SiO_4$ was detected at the coating profile adjacent to the mild steel substrate. In fact, there is extraordinary similarity in the dendritic morphologies observed in both cases, which also indicates that the solid solution lithium zinc iron silicates are formed by a diffusion controlled mechanism.

The formation of a solid solution can be explained by the similarity in the cation radii and the electron configuration of Fe^{2+} and Zn^{2+}, just as in the case of $Fe_yZn_{(1-y)}SiO_3$.

It is of value to mention that the XRD pattern of synthetic Li_2FeSiO_4 is inconsistent with previous results.[6] Considering that the set of peaks for the first crystallised phase in B3 glass, which contains no zinc oxide, can fit those of lithium zinc iron silicate very well, there are two interpretations. One is that, like Li_2ZnSiO_4, there exist several polymorphs of Li_2FeSiO_4. The second explanation is that, as a result of additional substitutions, the structure of lithium iron silicate is transformed to that of $LiZn_{(1-x)}Fe_xSiO_4$.

It is observed that the third crystallised phase in the heat treated iron-containing glasses, which exhibits a bright-contrast, dendritic morphology (Fig. 6), is associated with an XRD main peak of 2·99 d-spacing (Fig. 5). The EDX analysis indicated that the Fe/Si ratio was near 1. The brightness of such crystals in the back-scattered electron micrograph suggests that the lithium content within the crystals is quite low. Hence, it is probably a kind of iron silicate, inevitably with some substitutions as well. We have not succeeded in identifying this phase. However, judging from the fact that this is the major phase in crystallised B1 glass, in which the Fe^{2+}/Fe(total) ratio is much lower than that of B1 glass, it is suggested that this phase is possibly connected with Fe^{3+}.

The sheaf crystals, which are finally precipitated, give a set of XRD peaks which can be matched essentially to those of LF_2S_4, although there are some deviations resulting from substitution in the crystals. From EDX, the ratio of Fe/Si in the crystals is near 0·5.

4.2 Role of P_2O_5

The results in the present work indicate without exception that P_2O_5 plays an important role in the crystallisation of the iron-containing lithium silicate glasses.

The back-scattered electron micrograph of B1 glass containing 2·1% P_2O_5, which was crystallised at 820°C for 3 h (Fig. 6), shows a uniform and fine-grained structure throughout the sample, compared with the coarse-grained and cracked microstructure of crystallised B2 glass which possesses a similar composition to B1, but with less P_2O_5 at 1·1% (Fig. 6).

As the DTA traces illustrate (Fig. 3), although four exotherms are observed for each glass and B1 and B2 glasses exhibit the same sequence of crystallisation, the first exotherm for B2 glass, which is connected with the crystallisation of L(ZF)Sss, is rather low, almost merging with the quartz reference peak, compared with the clear first exotherm for B1 glass, suggesting that P_2O_5 mainly promotes the precipitation of L(ZF)Sss. Other evidence is that the DTA trace of B2 glass (Fig. 3), which contains twice as much P_2O_5 as B2 glass whilst maintaining the same molar relationship among other constituents, shows a sharp first exotherm due to the crystallisation of L(ZF)Sss. Consequently, a fine-grained microstructure was formed for B2 glass after heat treatment.

The deformation of the samples after heat treatment also provides some information about the rate of crystallisation. No appreciable deformation exists for B1 and B1′ samples heat treated at 820°C for 3 h, whereas the B2 sample has deformed significantly after the same process, which means that rapid crystallisation depends on the existence of sufficient P_2O_5.

B3 and B4 glasses with intermediate P_2O_5 content show intermediate results not only in the DTA traces (Fig. 3) but in the microstructure after heat treatment as well (Fig. 6).

It has been confirmed that quite small concentrations of P_2O_5 are effective in inducing the desired two-phase separation sometimes necessary for nucleation catalysis.[7,9] It is difficult to observe phase separation by SEM. However, back-scattered electron micrographs for the iron-containing glasses heat treated to 760°C (Fig. 6), show silica-rich globules dispersed in the iron-rich matrix. These may include previous phase-separated droplets which have merged into relatively large globules when crystallisation has taken place. The decrease of the thermal expansion coefficients for the iron-containing glasses heat treated at 580°C for 1 h may be indirect evidence for phase separation. The DTA scans for B1 samples heated previously in the range of ~530–580°C show a distinct decrease in the temperature of the first exotherm maximum. This may be further evidence that phase separation resulting from the low temperature nucleation treatment favours the crystallisation of L(ZF)Sss.

It is widely known that in lithium silicate glasses, Li_3PO_4 crystallites precipitate during the early stages of heat treatment and act as efficient nucleation sites for the crystallisation of lithium metasilicate[7,10] and that P_2O_5 has also been used as a nucleating agent in the crystallisation of lithia–zinc oxide–silica glasses. Its action may well be to form a crystalline phosphate phase which then nucleates an epitaxial silicate.[11] Since the structure of L(ZF)Sss is very similar to that of Li_2ZnSiO_4, and the structure of Li_2ZnSiO_4 is related to that of Li_3PO_4,[12] it is reasonable to suggest that L(ZF)Sss and LS are also nucleated by Li_3PO_4-type crystallites in the iron-containing glasses during heat treatment. The white cores existing in the globules (Fig. 6) are possibly the combination of such crystallites, but its brightness in the back-scattering electron micrograph indicates that it also contains some heavy elements, i.e. Fe, Zn.

The above considerations enable a tentative explanation for the beneficial effect of P_2O_5 to be put forward. The suggested mechanism is as follows. The small concentration of P_2O_5 induces extensive prior phase separation into silica-rich droplets dispersed in an iron-rich matrix and the formation of Li_3PO_4-type crystallites during heat treatment in the region of 580°C for 1 h. The interface between the two phases and the precipitated crystallites provide suitable sites for the nucleation of L(ZF)Sss and LS. Subsequently the droplets gradually merge into larger globules and the crystals start to grow from the previous nucleated sites while the temperature rises.

4.3 Influence of K_2O upon crystallisation

It has been reported that K_2O, which is present only in a small concentration in the glass, can be in some cases extremely important because it exerts an apparently disproportionate effect upon the crystallisation behaviour.[9] For example, it promotes the formation of lithium metasilicate in preference to the disilicate in photo-nucleated glass-ceramics.[9] It also changes the order of mineral formation and results in departure from equilibrium condition in the Li_2O–ZnO–SiO_2 system.[13] A similar effect of K_2O on the crystallisation behaviour in the iron-containing lithium silicate glasses was found in the present work.

Comparing the crystallisation sequences and the glass compositions of B1 and B2 with those of B3 and B4, it can be seen that a change in crystallisation sequence occurs such that LS precipitates as the second phase for B3 and B4 instead of quartz which

is the second crystallised phase for B1 and B2 glasses. The main differences between their compositions are that B3 and B4 glasses contain more K_2O and SiO_2 and less FeO and ZnO than B1 or B2 glasses. Differences in SiO_2 and FeO are considered unlikely to be the cause of crystallisation of LS in preference to quartz and the difference in ZnO concentration between the glasses is far less than that of K_2O. Therefore, the precipitation of LS is probably associated with the presence of more K_2O.

As a result of crystallisation, the residual glass is gradually enriched in K_2O and hence its viscosity reduces. Therefore, one possible mechanism for the change of the morphology of L(ZF)Sss from dendrites to small spherulites in B4 after extended high temperature treatment is that solution/reprecipitation occurs in the lower viscosity residual glass. Evidence for this is that there is no change in the nature of the crystal phase, and the samples have deformed significantly after long-term heat treatment.

4.4 Estimation of the distribution of crystallised phases in the glass-ceramic coating profile after heat treatment

It can be seen in Table 4 that there are marked differences in both the kinds and the amounts of the crystallised phases for B1, B2, B3 and B4 glasses after heat treatment. It is interesting to relate these results to the glass-ceramic coating profile adjacent to the mild steel substrate and compare them with the results of previous work.[5,6]

From the theory of X-ray diffraction for quantitative multicomponent analysis, it is known that for a specific (h k l) reflection from a component i in the X-ray powder diffraction pattern of a mixture, the intensity equation is[14]

$$I_i(\mathrm{h\,k\,l}) = K_i V_i / \alpha_t$$

where

K_i = constant for component i,
α_t = linear absorption coefficient of the total sample,
V_i = volume fraction of component i.

Although α_t varies with different samples, the relationship between the intensity and the volume fraction for any pair of components i,j in the same sample is

$$I_i/I_j = K_i V_i / K_j V_j = K V_i / V_j$$

Hence, the ratio of two special reflection intensities for two components provides some information on their relative amounts.

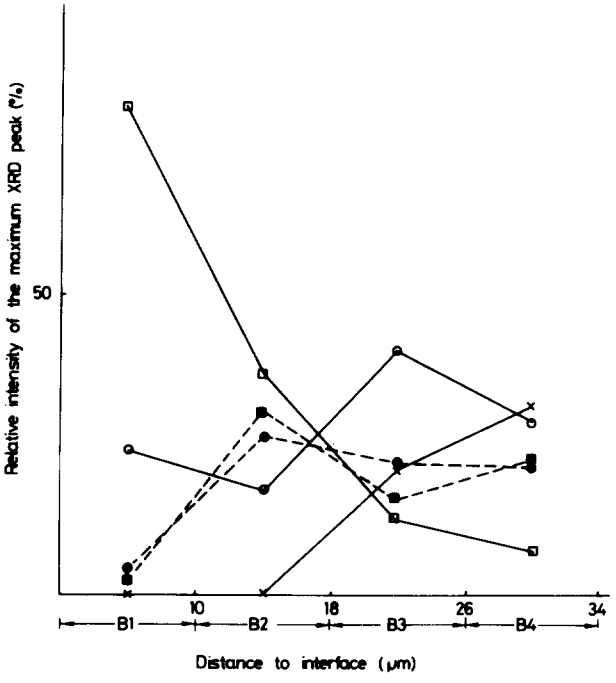

Fig. 8. Estimation of the distribution of crystalline phases in the coating profile heat treated at 820°C for 3 h. □, Quartz; ○, L(ZF)Sss; ×, LS; ●, FS; ■, LF_2S_4.

Figure 8 shows the relationship between the types of crystallised phases, as well as a rough estimate of their relative amounts, and their positions in the coating profile. The relative intensity of the maximum peak for each crystallised phase in glass having experienced the heat treatment identical to that for the glass-ceramic coating is plotted against the distance of the corresponding layer from the mild steel substrate.

The following conclusions can be seen from Fig. 8.

(1) In all regions of the profile, L(FZ)Sss always appears as a major phase. This is consistent with the results of the previous work, which showed that L(FZ)Sss dendrites formed at the interface and extended at most 4 μm into the fired-only coating. After heat treatment, the original dendritic growth extended to form a continuous layer between the substrate and the crystallised coatings.[5,6]

(2) Quartz exists as a major phase in the glass-ceramic coating profile immediately adjacent to the substrate, but its amount decreases rapidly with increasing distance into the coating. It not only confirms the suggestion in the previous work that quartz crystallised in the coating but also provides more detailed information for its distribution in the coating profile.

(3) LS crystallises as a major phase instead of

quartz in the region of 18–34 μm away from the interface.

(4) As a result of the presence of Fe(III), FS and LF_2S_4 appear in the crystallised bulk glasses but they are unlikely to be present in the real glass-ceramic coating profile, since the majority of iron content was reported to be in the form of Fe(II).[5,6] It is evident that the greater the Fe(II)/Fe total ratio, the more L(FZ)Sss forms instead of FS and LF_2S_4. Such a deduction is in agreement with the results of previous work.[5,6]

Although the investigation of the crystallisation behaviour of the bulk glasses does provide supplementary information for the glass-ceramic coating, there is some deviation of the bulk glasses from the real coating, either in the types or in the morphology of the crystals. This is mainly for the following reasons.

(1) As shown earlier, the ratios of Fe(II)/Fe(total) for the bulk glasses are lower than that of the real coating profile.
(2) There is actually a continuous change in the compositional gradient in the coating with firing and heat treatment time.
(3) The bulk samples and coating differ in both physical form and thermal history, for the coating process starts from a glass powder and initially experiences a firing stage.
(4) The assumption of a constant lithium/silicon ratio may introduce some error, for there is evidence of an enrichment of lithium oxide in the interface region.[5,6]

4.5 Thermal expansion characteristics and the estimation of the stress distribution in the coating profile

It is accepted that a glass-ceramic is a composite material and its thermal expansion coefficient is a function of the expansion coefficients and elastic properties of all the phases present.[9] Comparing the thermal expansion behaviour (Table 5) and crystallised phases (Figs 5 and 8) for all the glasses at different stages of heat treatment leads to the following conclusions.

(1) The decrease in thermal expansion coefficient for all glasses treated at 580°C for 1 h is associated with change in nucleation, probably caused by preliminary phase separation.
(2) The increase of expansion coefficient for B1 and B2 samples with increasing heat treatment temperature and time are closely connected with the increasing amount of quartz.
(3) By comparing the expansion coefficients for all glasses having received the initial stage of heat treatment in which L(FZ)Sss exists as the major crystalline phase, it can be deduced that the expansion coefficient for L(FZ)Sss is comparatively low. This suggestion has been confirmed by the measurement of the thermal expansion coefficient for the synthetic $LiFe_{0.5}Zn_{0.5}SiO_4$, in which a value of 7·73 MK^{-1} was obtained.
(4) The high value of the expansion coefficient for B4 glass can be interpreted by the higher concentration of K_2O compared with the other glasses. Moreover, judging from the lower value of the expansion coefficient for B4 glass treated at 820°C for 3 h in which LS, FS and LF_2S_4 are the major phases instead of quartz, it can also be concluded that the expansion coefficients for these phases are not as high as that of quartz.

It is of great interest to estimate the stress distribution in the coating profile using the observed thermal characteristics of the crystallised bulk glasses.

It is known that the stress set up at the interface between the coating and the substrate is proportional to the difference in the thermal expansion coefficients thereof, and a slight compressive stress is required for ceramic coating so as to achieve optimum coating properties.[15] It is of value to note that the thermal expansion coefficients for B1, B2, B3 and B4 samples whose compositions correspond to the different diffusional layers adjacent to the mild steel substrate and which have experienced the heat treatment identical to that for the glass-ceramic coatings, are 15·2, 10·2, 9·36 and 9·46 MK^{-1}, respectively. If we compare them with those of the mild steel (12·4 MK^{-1}) and the normal glass-ceramic coating (13·2 MK^{-1}), it can be found that in the region of 2–10 μm immediately adjacent to the substrate there exists a marked tensile stress which is

Table 5. Thermal expansion coefficients (MK^{-1}) of glass before and after different stages of heat treatment (50°C–400°C)

Glass	*Before heat treatment*	*After different stages of heat treatment*			
		A	*C*	*D*	*E*
B1	9·09	8·26	11·9	15·3	15·2
B2	9·21	8·56	8·32	9·86	10·2
B3	8·82	9·66	9·21	11·0	9·36
B4	10·1	9·83		9·58	9·46
B	7·8				13·2

unfavourable to optimum coating properties. However, compressive stress will be set up towards the outer surface of the coating, suppressing flaw propagation there. Hence, a proper adjustment is necessary for setting up a slight compressive stress in the glass-ceramic coating adjacent to the mild steel substrate so as to improve the coating properties.

5 Summary and Conclusions

Volume crystallisation occurs during heat treatment of a group of lithium iron silicate glasses which have compositions corresponding to the different layers in the glass-ceramic coating composition profile.

The four glasses chosen show two different kinds of crystallisation sequences. In the case of B1 and B2 glasses, L(ZF)Sss, quartz, FS and LF_2S_4 precipitate successively during heat treatment. For B3 and B4 glasses, LS replaces quartz as the second crystallised phase in the crystallisation sequence. However, although it is difficult to associate the crystallisation of quartz with an individual exotherm in the DTA scans for B3 and B4 glasses, there is still a small amount of quartz appearing during the heat treatment.

L(ZF)Sss solid solutions can occur over a wide Fe/Zn ratio. Their XRD patterns have been identified as being similar to that of Li_2ZnSiO_4.

P_2O_5 is an effective nucleating agent for the crystallisation of the lithium iron silicate glasses. Its action is probably to induce extensive prior phase separation into silica-rich droplets in an iron-rich matrix and the formation of Li_3PO_4-type crystallites during the low temperature heat treatment, then the interface between the two phases and the precipitated crystallites provide suitable sites for the nucleation of L(ZF)Sss and LS.

The increase of the concentration of K_2O in B3 and B4 glasses causes the change of their crystallisation sequence and favours the formation of LS.

The investigation of the crystallisation behaviour for the bulk lithium iron silicate glasses suggests that the major crystalline phases in the glass-ceramic coating immediately adjacent to the mild steel substrate are L(ZF)Sss and quartz. However, in the region ~ 18–$34\,\mu m$ away from the interface, LS occurs as a major phase instead of quartz.

The increase in the thermal expansion coefficient of the lithium iron silicate glasses is closely connected with the formation of increasing amounts of quartz with increasing heat-treatment temperature and time. Therefore, a close control of the heat treatment is necessary in order to set up a slight compressive stress in the glass-ceramic coating adjacent to the mild steel substrate so as to achieve optimum coating properties.

Acknowledgements

The author should like to thank his colleagues in the Centre for Advanced Materials Technology for their assistance and helpful discussion, and also to thank the Physics Department and Ceramic Developments (Midlands) Limited for providing financial support.

References

1. Maskell, K. H. & White, D., *Vitreous Enamelling: A Guide to Modern Enamelling Practice*, The Institute of Ceramics, Pergamon Press, Oxford, 1986.
2. Onyshkevych, L., *Ceram. Eng. Sci. Proc.*, **2**(3–4) (1981) 166.
3. King, B. W., Tripp, H. P. & Duckworth, W. H., *J. Am. Ceram. Soc.*, **42** (1959) 504.
4. Healy, J. H. & Andrew, A. J., *J. Am. Ceram. Soc.*, **34**(7) (1951) 207.
5. Sturgeon, A. J., Glass-ceramic coating metals. PhD thesis, Warick University, UK, 1987.
6. Sturgeon, A. J., Holland, D., Partridge, G. & Elyard, C. A., *Glass Technol.*, **27**(3) (1986) 102.
7. Hammetter, W. F. & Loehman, R. E., *J. Am. Ceram. Soc.*, **70**(8) (1987) 577.
8. Maxwell, C. J. & Brungs, M. P., *Glass Technol.*, **25**(5) (1984) 244.
9. Mcmillan, P. W., *Glass-Ceramics*, Academic Press, London, 1979.
10. Dupree, R., Holland, D. & Mortuza, M. G., *Physics and Chemistry of Glasses*, **29**(1) 15–21.
11. West, A. R. & Glasser, F. P., *J. Mater. Sci.*, **5**(7) (1970) 676.
12. Trotter, J., *Structure Report*, 47(A), D. Reidel Publishing Company, Utrecht, 1982.
13. Petrova, F. H., *J. Appl. Chem. (Leningrad)*, **48**(8) (1975) 1683. (In Russian.)
14. Chung, F. H., *Advances in X-ray Analysis*, Vol. 17, Plenum Press, New York, 1974, p. 106.
15. Duke, D. A. *et al.*, *J. Am. Ceram. Soc.*, **51** (1968) 98.